MHD Fluctuations in the Heliosphere

B. Bavassano and R. Bruno

Abstract The solar wind is an excellent laboratory to study the MHD turbulence behaviour in a collisionless plasma. This is a fundamental topic for both plasma physics and astrophysics. The impressive amount of observations at different solar distances and latitudes collected in the last decades has allowed us of reaching a good understanding on many aspects of the complex phenomenon of the solar wind variability at MHD scales. Here we discuss the character of the observed fluctuations and focus on their radial evolution as the plasma flow expands into the interplanetary space. A comparison is performed between fluctuations seen in low- and high-latitude solar wind. Implications about processes of local generation of turbulence are discussed.

Key words: Interplanetary physics (MHD waves and turbulence; Sources of the solar wind) – Space plasma physics (Turbulence)

1 Introduction

The heliosphere is the region of space influenced by the Sun through its expanding corona, the solar wind. This is a collisionless plasma flow that offers one of the best opportunities to study plasma phenomena by in-situ measurements. Here we will focus on a topic of primary importance for both plasma physics and astrophysics, the magnetohydrodynamic (MHD) turbulence. The use of the term MHD only refers to the fact that we are looking at phenomena falling in the MHD regime (i.e., frequency well below the pro-

B. Bavassano, R. Bruno
Istituto di Fisica dello Spazio Interplanetario (Istituto Nazionale di Astrofisica)
Via del Fosso del Cavaliere 100, 00133 - Roma, Italy
e-mail: Bruno.Bavassano@ifsi-roma.inaf.it, Roberto.Bruno@ifsi-roma.inaf.it

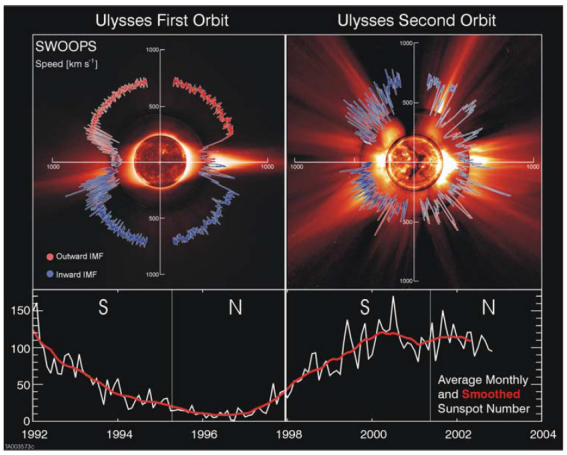

Fig. 1 Polar plots of the solar wind speed as a function of latitude for the Ulysses' first two orbits. Sunspot numbers (bottom panel) show that the first orbit occurred through the solar cycle declining phase and minimum while the second orbit spanned solar maximum (adapted from [30], copyright 2003 American Geophysical Union, modified by permission of American Geophysical Union).

ton gyrofrequency). The name does not imply that these phenomena may necessarily be described by the MHD theory.

The three-dimensional structure of the solar wind is strongly dependent upon the solar cycle. As shown in Fig. 1, at low solar activity the solar wind is characterized by a bimodal structure [28], with a steady, fast wind at high latitudes and a slower and more variable wind at low latitudes. Conversely, at high solar activity highly variable flows are observed at all latitudes and the wind structure appears to be a complicated mixture of flows [30]. However, this state with variable flows at all heliographic latitudes is a short-lived feature of the heliosphere. After the reversal of the solar magnetic field, a recovery of the winds bimodal structure begins quite soon [29]. The fast high-latitude wind (polar wind) and the low-latitude wind come from different sources. The fast wind is from coronal holes, while slow wind flows from open magnetic flux-tubes in the streamer belt region.

The solar wind is a plasma with extremely low viscosity and resistivity. Both kinetic and magnetic Reynolds numbers, which essentially measure the relative weight of nonlinear and dissipative terms in the MHD equations, are high. Thus, relevant turbulent effects have to be expected. As well known, the solar wind turbulence strongly affects several aspects of the heliospheric behaviour, such as plasma heating, solar wind generation, particles acceleration, and cosmic rays propagation. Recently it has been shown [16] that the turbulence is also able to influence the geomagnetic activity.

In the seventies and eighties impressive advances have been made in the knowledge of turbulent phenomena in the solar wind [39]. In those years, however, with spacecraft observations confined within a small latitudinal belt around the solar equator, only a limited fraction of the heliosphere was accessible. In the nineties, whith the launch of Ulysses, the first spacecraft with a highly inclined orbital plane with respect to the ecliptic, the investigations have been extended to high-latitude regions of the heliosphere. This has al-

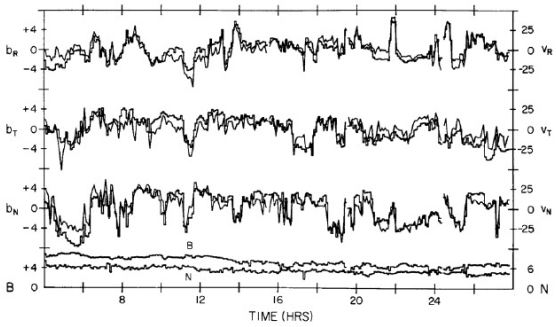

Fig. 2 One of the first observations of Alfvénic fluctuations (adapted from [9], 1971, copyright 1971 American Geophysical Union, modified by permission of American Geophysical Union).

lowed of studying how the MHD turbulence evolves in polar solar wind, a plasma flow in which the effects of large-scale inhomogeneities are considerably less important than in low-latitude wind. With this new laboratory relevant advances in interplanetary turbulence have been made [11, 20].

2 Alfvénic Fluctuations

Since the first observations (e.g., [9, 15]) it it was recognized that the solar wind MHD fluctuations have a strong Alfvénic character (Alfvénic modes have a much longer lifetime than other MHD modes [1]). An example is shown in Fig. 2, with highly correlated variations in velocity and magnetic field (and almost constant density and magnetic field magnitude).

It is useful to briefly recall some of the parameters that are generally used to describe Alfvénic fluctuations. Basic quantities are the Elsässer's variables $\mathbf{z}_\pm = \mathbf{v} \pm \mathbf{b}$ (e.g., see [39]), that are ideally suited to extract an Alfvénic signal from velocity and magnetic field measurements. Here $\mathbf{v}$ and $\mathbf{b}$ are the velocity and magnetic field vectors, respectively, with the magnetic field $\mathbf{b}$ scaled to Alfvén units (i.e., divided by $\sqrt{4\pi\rho}$, with ρ the mass density). Taking into account how the sign of the Alfvénic correlation depends on the propagation direction with respect to the background magnetic field, it has become common to use the above definition for a background magnetic field pointing to the Sun, while the equation $\mathbf{z}_\pm = \mathbf{v} \mp \mathbf{b}$ is taken for the opposite polarity. With this choice we have that, whatever the magnetic polarity is, $\mathbf{z}_+$ ($\mathbf{z}_-$) fluctuations always correspond to modes with an outward (inward) direction of propagation, with respect to Sun, in the plasma frame. The relative weight of the energies (per unit mass) e_+ and e_- associated to $\mathbf{z}_+$ and $\mathbf{z}_-$ fluctuations, respectively, is measured by the Elsässer ratio $r_E = e_-/e_+$. An analogous measure for the energies e_V and e_B of the $\mathbf{v}$ and $\mathbf{b}$ fluctuations is given by the Alfvén ratio $r_A = e_V/e_B$. Other related parameters are the normalized cross-helicity $\sigma_C = (e_+ - e_-)/(e_+ + e_-) = (1 - r_E)/(1 + r_E)$ and the normalized residual energy $\sigma_R = (e_V - e_B)/(e_V + e_B) = (r_A - 1)/(r_A + 1)$.

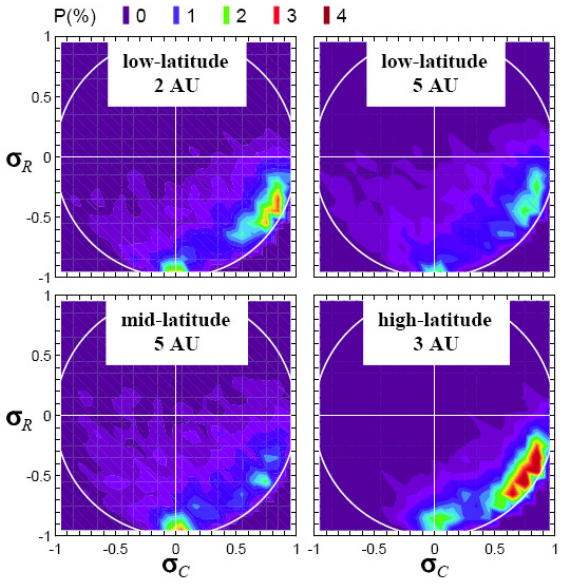

Fig. 3 Occurrence frequency distributions in the σ_C-σ_R plane (modified from [4], copyright 1998 American Geophysical Union, by permission of American Geophysical Union).

Both outward and inward propagating fluctuations are observed in the solar wind. Outward fluctuations mainly have a solar origin (or, more precisely, inside the Alfvén critical point). Conversely, inward fluctuations can only be generated outside such critical distance. As well known, the presence of both kinds of fluctuation leads to the development of nonlinear interactions.

3 Magnetic Variations

As first discussed by [4], when solar wind fluctuations are analysed in terms of σ_C and σ_R and occurrence frequency distributions are displayed in a σ_C-σ_R plane, it clearly appears that the peak at high σ_C due to the Alfvénic population is accompanied by an extended tail towards the region close to σ_C=0 and σ_R=−1, with a secondary peak at the end caused by fluctuations essentially of magnetic type. Fig. 3 indicates that this is a quite general feature, observed for all kinds of solar wind regime [4]. The radial expansion of the solar wind plays a role in this two-population scheme [2, 13], with an increasing weight of the magnetic fluctuations. Moreover, it has been shown [2] that the magnetic population, even when of secondary importance in terms of occurrence frequency, may correspond to a primary peak in the distribution of total (magnetic plus kinetic) energy. Thus, from the point of view of the energy content of solar wind fluctuations the magnetic population appears able to play a primary role. Finally, for the magnetic population fluctuations

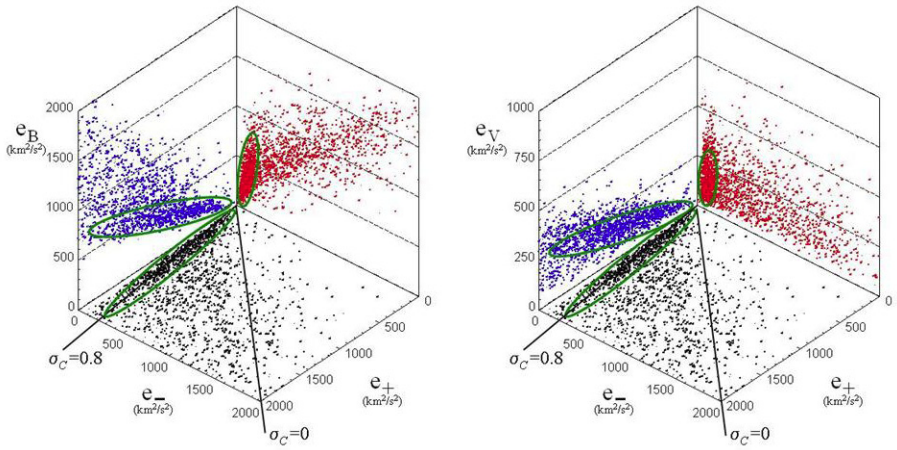

Fig. 4 3-D plots of fluctuation energy values in the polar wind. An e_+-e_--e_B frame is used at left and an e_+-e_--e_V frame at right (note that e_B and e_V axes have different scales). Dots of different colours indicate projections on the coordinate planes. Lines for σ_C=0.8 and σ_C=0 are shown in the plane e_+-e_-.

are more planar, in a plane perpendicular to the background magnetic field, than those for the Alfvénic population. This is reminiscent of quasi-two-dimensional fluctuations [25]. Yet, this kind of geometry may well come from coronal magnetic flux tubes that, turbulently mixed, are swept out by the solar wind [2].

3-D plots of the fluctuation energy values are shown in Fig. 4. In addition to the highly populated clouds indicated by green ovals, that correspond to outward propagating Alfvénic fluctuations, a broad population extending towards higher magnetic energies (e_B) and lower cross-helicity (σ_C) is clearly apparent in the left plot. The same does not hold for e_V (right plot). All this confirms that solar wind fluctuations are a mixture of an Alfvénic population and a magnetic population. For this last one the values of e_B are significantly above the levels typically observed for the Alfvénic population.

In a complementary approach, it is interesting to investigate the role that the two populations have in building the distributions of magnetic and kinetic energies. For the same data of Fig. 4 such distributions have been derived separately for four ranges of σ_C and compared to that obtained from the whole sample. The results (Fig. 5) show that the e_B and e_V distributions respond in a different way to a change in the σ_C range. While for the kinetic energy (right) the various curves have similar shapes, for the magnetic energy (left) significant differences are observed. In particular, Alfvénic fluctuations (σ_C above 0.6, red) are mainly responsible for the peak of the overall distribution (black), while non-Alfvénic fluctuations (σ_C from -0.1 to 0.3, blue) are dominant in the extended (high-e_B) tail. In other words, the peak and

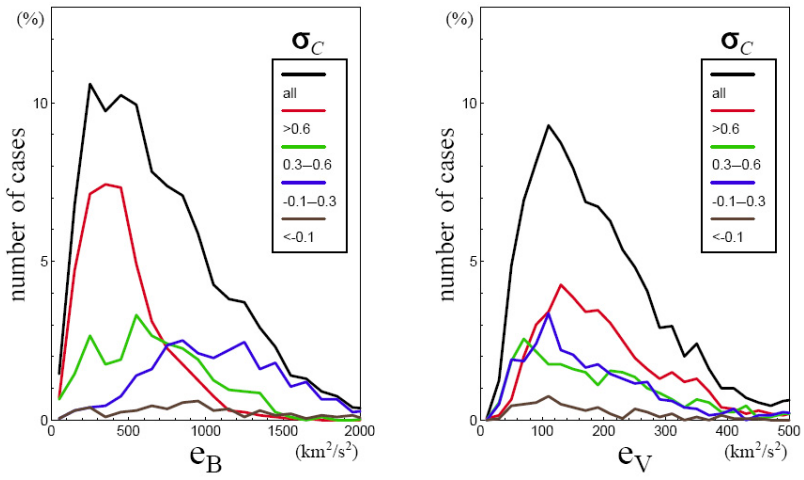

Fig. 5 Histograms of e_B (left) and e_V (right) for different ranges of σ_C.

the tail of the e_B distribution have a different Alfvénic content or, in general, a different nature.

4 Turbulence in Low-Latitude Wind

Since the first studies on Alfvénic fluctuations in ecliptic wind (e.g., see [9]) it was realized that fast streams (or, more precisely, their trailing edges) were the best places to observe them. In those years (mid-seventies) a hot topic was that of the turbulence generation and evolution. Observations at different heliocentric distances are crucial to this kind of study. The launch of Helios

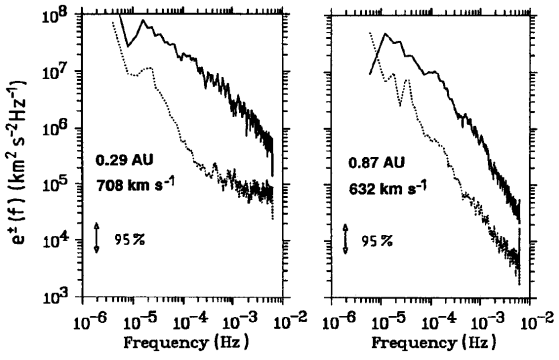

Fig. 6 Power spectra of e_+ and e_- (solid and dotted line, respectively) in the trailing edge of fast streams at 0.29 and 0.87 AU (adapted from [24], copyright 1990 American Geophysical Union, modified by permission of American Geophysical Union).

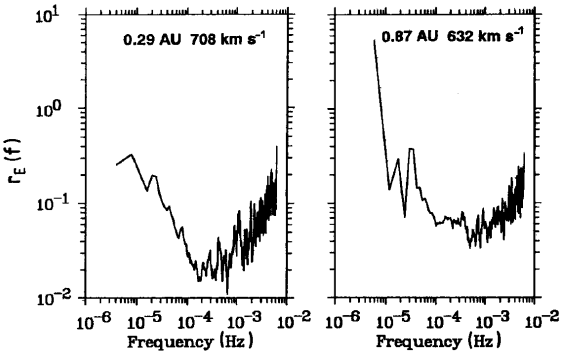

Fig. 7 Power spectra of the Elsässer ratio r_E ($= e_-/e_+$) for the same data of Fig. 6 (adapted from [24], copyright 1990 American Geophysical Union, modified by permission of American Geophysical Union).

1 and 2 (in December 1974 and January 1976, respectively), systematically covering the inner heliosphere from 0.3 to 1 AU, combined with a very stable pattern of the interplanetary medium (in a period of low solar activity) allowed to get the first evidence about a radial evolution of the solar wind turbulence [3, 17]. In the next years, with a boom of studies on this subject, impressive advances were made.

Fig. 6 shows how e_+ and e_- power spectra (solid and dotted line, respectively) vary when solar distance increases from 0.3 to 0.9 AU [24]. The e_+ spectrum declines faster than that of e_-, with the result that the two spectra approach each other. At the same time the spectral slopes evolve in such a way that an extended inertial regime expands to low frequencies.

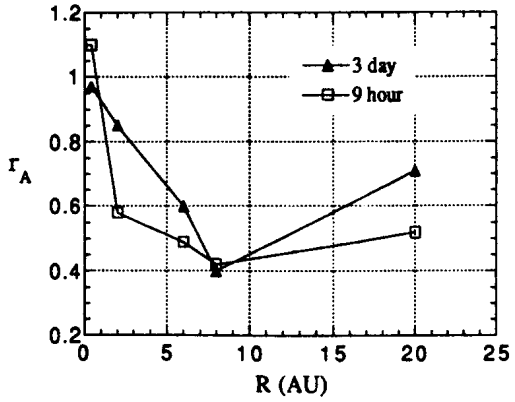

Fig. 8 Radial variation of the Alfvén ratio r_A ($=e_V/e_B$) as seen by Helios and Voyagers between 0.3 and 20 AU (adapted from [33], copyright 1990 American Geophysical Union).

The corresponding variation in the relative weight of outward and inward fluctuation energies is shown in Fig. 7 [24]. The very small values of r_E observed at 0.3 AU in the core of the Alfvénic regime (frequencies around $10^{-4} - 10^{-3}$ Hz) have disappeared at 0.9 AU. However, the predominance of $\mathbf{z}_+$ fluctuations remains a strong feature of the Alfvénic turbulence observed

by Helios in fast streams inside 1 AU. Ulysses data from the ecliptic phase of the mission have shown that this situation persists at least up to 5 AU [6].

A relevant feature of the solar wind turbulence is that the magnetic energy tends to become dominant as the solar distance increases. This decreasing trend for the Alfvén ratio r_A ($=e_V/e_B$) clearly appears in Helios data [12, 24]. The r_A decrease, however, is not without a limit. This is seen in Fig. 8, that combines Helios and Voyagers observations to give an overall view of the radial variation of r_A between 0.3 and 20 AU [33]. The 9-hr curve (squares), the one of the two reported curves that best describes the typical MHD scales, shows that r_A, after a fast and pronounced decrease, remains nearly unchanged.

5 Turbulence in Polar Wind

As already mentioned, Ulysses observations have shown that, at low solar activity, the solar wind at high latitudes is a fast and relatively steady flow (e.g., [28]). A remarkable feature of the polar wind is the ubiquitous presence of an intense flow of Alfvénic fluctuations (e.g., [19, 21, 37, 4]). Similar to previous ecliptic observations in fast streams, a largely dominant fraction of these fluctuations is outward propagating, with respect to the Sun, in the solar wind frame. The polar wind, a flow in which large-scale inhomogeneities are almost absent, offers the best opportunity to study the turbulence evolution under nearly undisturbed conditions (with respect to low-latitude wind).

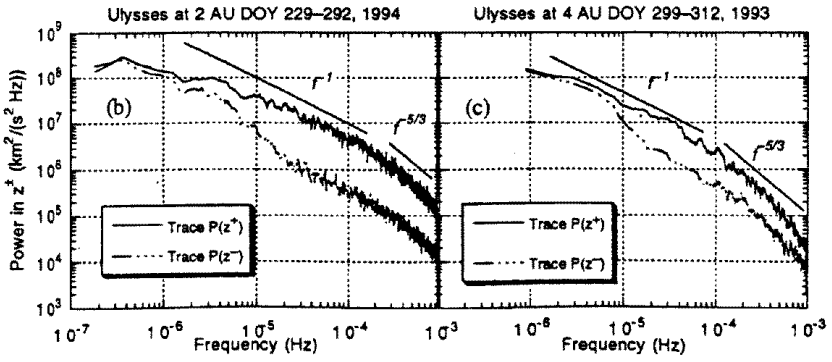

Fig. 9 Power spectra of $\mathbf{z}_+$ and $\mathbf{z}_-$ (upper and lower curve, respectively) in polar wind at (left) $\sim$ 2 AU and (right) $\sim$ 4 AU (adapted from [19], copyright 1995 American Geophysical Union, modified by permission of American Geophysical Union).

Fig. 9 shows polar wind spectra of $\mathbf{z}_+$ and $\mathbf{z}_-$ at distances of about 2 and 4 AU from the Sun [19]. The spectral evolution appears qualitatively similar

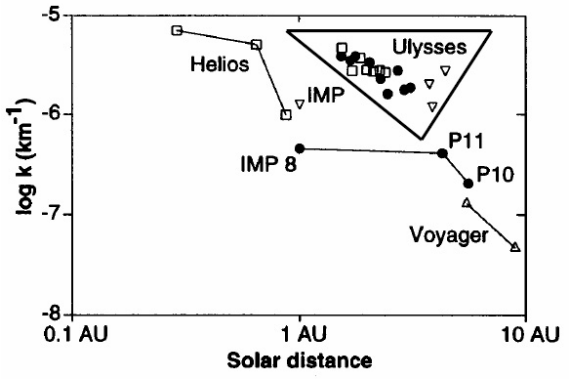

Fig. 10 Variation of the spectral breakpoint with radial distance. Data inside the upper triangle are for high-latitude observations by Ulysses, while the other data are from spacecraft near the ecliptic (adapted from [22], copyright 1996 American Geophysical Union, modified by permission of American Geophysical Union).

to that observed in low-latitude fast streams, with the development of a turbulent cascade with increasing distance that moves to lower frequencies the breakpoint between the f^{-1} and $f^{-5/3}$ regimes. However, as shown by Fig. 10, for polar wind the breakpoint is at smaller scale than at similar distances in low-latitude wind [22]. Thus, spectral evolution in polar wind is slower than at low latitudes.

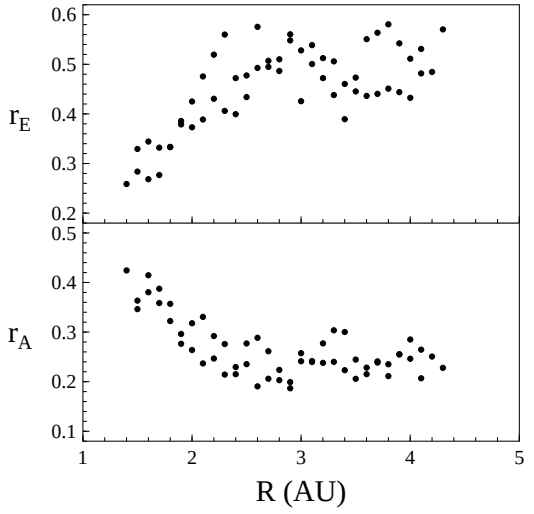

Fig. 11 Radial variation of (top) the Elsässer ratio r_E ($=e_-/e_+$) and (bottom) the Alfvén ratio r_A ($=e_V/e_B$) in polar wind.

A general agreement exists about the fact that the slower evolution for polar turbulence has to be ascribed to the lack of a large-scale stream structure. The role of such a structure in accelerating the turbulence evolution has been stressed by [4] using Ulysses data at mid-latitudes with strong gradients in the wind velocity. It should be also mentioned that the turbulence appears

younger in polar flow, since fluctuations at a given distance have had less time to evolve due to the higher wind speed (e.g., see [26]).

The radial variation of the Elsässer ratio r_E and the Alfvén ratio r_A in polar wind is shown in Fig. 11. Both trends, increasing for r_E and decreasing for r_A, do not go beyond some limits, in agreement with low-latitude observations.

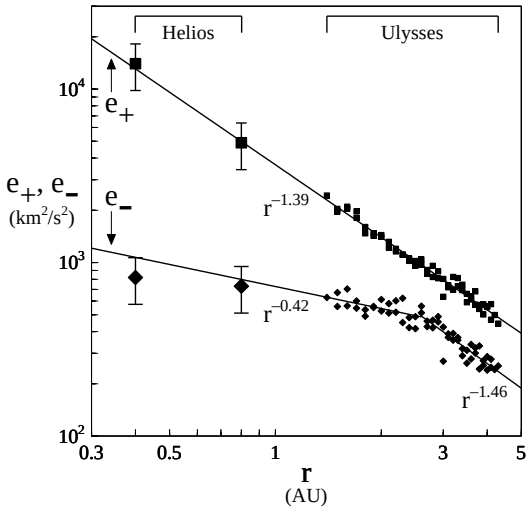

Fig. 12 A composite plot combining Ulysses observations in polar wind with those by Helios 1 and 2 inside 1 AU in the ecliptic plane (adapted from [5], copyright 2000 American Geophysical Union, modified by permission of American Geophysical Union). The values of e_+ (e_-) are shown as squares (diamonds), small for Ulysses and large for Helios. Best fit lines and radial power laws for Ulysses data are given.

Fig. 12 combines Ulysses observations in the polar wind with those by Helios 1 and 2 within the trailing edge of low-latitude fast streams at about 0.4 and 0.8 AU [5]. As regards the polar wind, the e_+ values exhibit the same radial gradient over all the investigated range of distances, while for e_- a change of slope around 2.5 AU is clearly apparent. A remarkable point is that the Ulysses best fit lines are in good agreement with the Helios data.

6 Solar Wind Turbulence Models

A well established property of the Alfvénic turbulence is that, in the presence of an energy imbalance between $\mathbf{z}_+$ and $\mathbf{z}_-$ modes, the non-linear interactions act in such a way to lead the turbulence towards a state in which the only left modes are those initially prevailing [18]. In this so-called aligned state the minority component has completely disappeared and a total alignment between velocity and magnetic fluctuations has been established. In the case of solar wind, even though an energy imbalance in favour of outgoing $\mathbf{z}_+$ modes exists, the turbulence does not end with an aligned state. The only way to

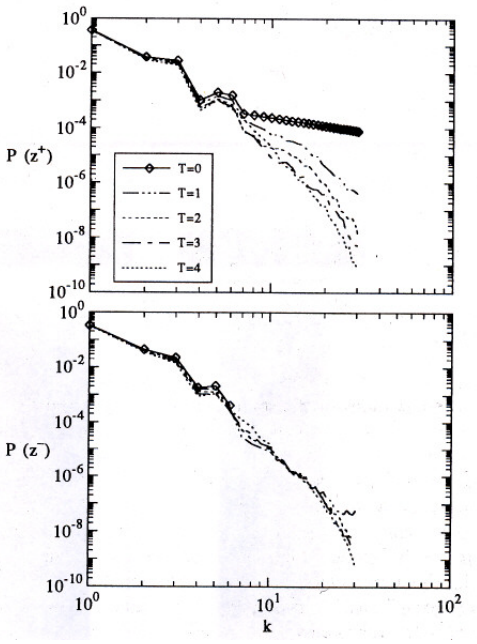

Fig. 13 Evolution of $\mathbf{z}_+$ (top) and $\mathbf{z}_-$ (bottom) power spectra as driven by a velocity shear (adapted from [34], copyright 1991 American Geophysical Union, modified by permission of American Geophysical Union). Time evolution in the simulation corresponds to radial evolution in the solar wind, with T=3 roughly equivalent to 1 AU.

avoid the disappearance of the minority ingoing $\mathbf{z}_-$ modes is that one or more processes act to refill the solar wind with that kind of mode.

Several models have been proposed for turbulence generation in the interplanetary space. Both non-linear processes at velocity gradients and plasma instabilities have been invoked to drive the turbulence evolution. The interaction between Alfvénic fluctuations and convective solar wind structures has also been considered. Velocity gradients are certainly relevant in low- and mid-latitude wind, while in polar wind other processes could be of primary importance, with a robust candidate represented by the parametric decay. Some of the most popular models for turbulence generation and evolution in the different solar wind regimes will be now discussed.

6.1 Models for Low-Latitude Turbulence

Velocity gradients can generate turbulence and drive the radial evolution of $\mathbf{z}_+$ and $\mathbf{z}_-$ spectra. In Fig. 13 the results of a simulation [34] are shown (for other references on this subject see [39]). The velocity shear leads to an approximately equal injection of power in $\mathbf{z}_+$ and $\mathbf{z}_-$ at large scale. Starting with essentially no power for $\mathbf{z}_-$ at high wavenumbers, this injection leads to a $\mathbf{z}_-$ spectrum that quickly grows until is balanced by dissipation. Thus, the $\mathbf{z}_-$ spectrum is already well developed near the Sun. In contrast, the

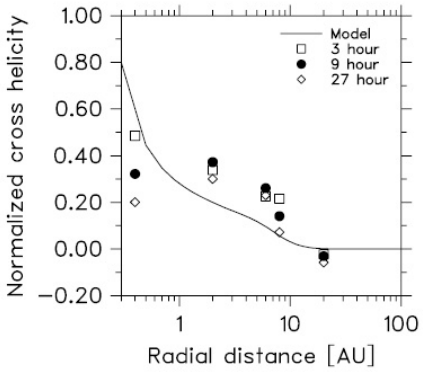

Fig. 14 The radial variation of the normalized cross-helicity as modeled by [27] is compared to observations by Helios (inside 1 AU) and Voyagers (adapted from [27], copyright 2004 American Geophysical Union, modified by permission of American Geophysical Union).

injection of $\mathbf{z}_+$ is inadequate to balance the dissipation of initially strong $\mathbf{z}_+$ fluctuations. Thus, the $\mathbf{z}_+$ spectrum decreases rapidly. Subsequently, when the $\mathbf{z}_+$ level is close to that of $\mathbf{z}_-$, the two spectra gradually evolve toward each other. This is strongly reminiscent of the spectra variation observed by Helios in the inner heliosphere. The simulations also indicate that magnetic field reversals, common in low-latitude wind, speed up the evolution.

More recently the cross-helicity radial decrease has been modeled as caused by velocity gradients and pickup-ion effects [27]. Velocity gradients drive large-scale nonlinear Kelvin-Helmholtz instabilities that inject kinetic energy only (hence without contributions to cross-helicity, that would request also a magnetic term). As regards pickup ions, in the outer heliosphere they encounter an approximately transverse magnetic field and therefore couple equally to both $\mathbf{z}_+$ and $\mathbf{z}_-$. Thus, driving supplies energy but not cross-helicity. In Fig. 14 the model predictions are compared to the observational data, as obtained by Helios and Voyagers inside and outside 1 AU, respectively. The model accounts reasonably well for the observed radial trend of σ_C, in other words driving by velocity shear and pickup-ions appears able to overcome the inherent tendency for MHD turbulence to produce aligned Alfvénic states.

An alternative way of describing the radial evolution of solar wind Alfvénic fluctuations is that proposed by [38], based on a two-component model (see also [35, 36]). In this approach the fluctuations are described as a mixture of 1) Alfvén waves, created near the coronal base and propagating outward along the magnetic field lines, and 2) static magnetic structures convected by the expanding solar wind. A comparison between predicted and observed radial trends for e_+, e_-, σ_C, and r_A is done in Fig. 15. In spite of the data dispersion a reasonable agreement appears to exist.

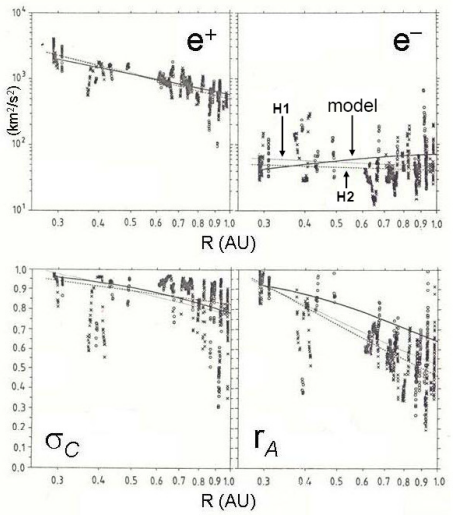

Fig. 15 Predictions (heavy lines) of the two-component (waves plus magnetic structures) model [38] are compared to the radial trends observed by Helios 1 and 2 (light lines) inside 1 AU (adapted from [38], copyright 1993 American Geophysical Union, modified by permission of American Geophysical Union).

6.2 Models for Polar Turbulence

Though weaker than in low-latitude wind, polar wind velocity gradients could still give a non-negligible contribution in generating turbulence. However, it is very likely that other processes take a leading role, with the parametric decay as the most robust candidate.

As regards velocity gradients, the occurrence of cross-helicity decreases in connection with polar wind microstreams was pointed out by [31]. Recently, the above model based on velocity gradients and pickup-ion effects [27] has been adapted to polar wind conditions [10]. Using lower shear, higher wind speed, and lower density, a reasonable tuning of the model parameters is able of leading to solutions behaving in a way comparable to that of the Ulysses observations (Fig. 16).

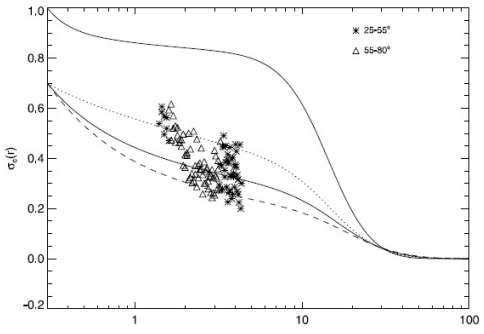

Fig. 16 The normalized cross-helicity at high latitudes as modeled by [10] is compared to Ulysses observations. The different curves are for different conditions at the inner boundary (adapted from [10], copyright 2005 American Geophysical Union, modified by permission of American Geophysical Union).

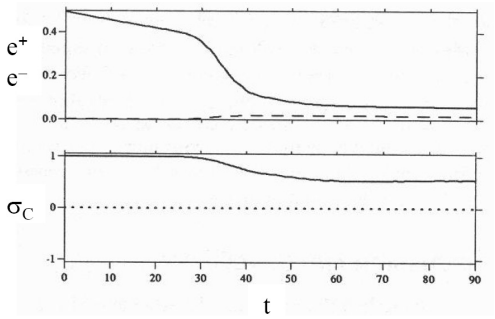

Fig. 17 Time evolution of e_+ and e_- (top, solid and dashed lines, respectively) and σ_C (bottom) for a parametric decay with $\beta = 1$, as modeled by [23] (adapted from [23], copyright 2000 American Geophysical Union, modified by permission of American Geophysical Union).

As for the parametric decay, it has been proposed (e.g., see review [8]) that a relevant role in driving the cross-helicity evolution in polar wind can be played by this process (an Alfvénic wave decay that essentially transfers energy to a backward Alfvénic mode and to a compressive mode). Simulations for the case of large-amplitude non-monochromatic Alfvénic fluctuations [23] have shown that the final state strongly depends on the value of β (thermal to magnetic pressure ratio). For $\beta < 1$ the normalized cross-helicity σ_C decreases, from an initial value of 1, to values close to 0. Thus, the instability appears able to completely destroy the initial Alfvénic correlation. In contrast, for $\beta = 1$ (a value closer to real solar wind conditions) σ_C remains different from 0 in the final state. In this case the parametric instability is not able to go beyond some limit in the disruption of the initial correlation between velocity and magnetic field fluctuations. This kind of solution, shown in Fig. 17, is reminiscent of the radial trend seen by Ulysses.

7 Final Remarks

The heliosphere is the only region of space in which in-situ measurements of particles and fields have been performed. This offers a unique opportunity for studying fundamental processes common to astrophysics and plasma physics (for instance, magnetic reconnection, particle acceleration, turbulence generation, plasma heating). Here we have discussed MHD fluctuations observed in the solar wind, a plasma flow resulting from the expansion of the solar corona. The solar wind is an excellent laboratory to investigate processes in a collisionless plasma.

In the above sections it has been shown that solar wind fluctuations at MHD scales have a strong Alfvénic component, with a predominance of fluctuations traveling (in the plasma frame) away from the Sun. However, non-negligible contributions to the wind variability also come from variations of magnetic type. All occurs in close-to-balance conditions between thermal and magnetic pressures (e.g., see [8, 40]).

Interplanetary, or local, generation of fluctuations is seen to overcome the inherent tendency for MHD turbulence to produce aligned Alfvénic states. The main candidates for solar wind turbulence driving are velocity gradients and parametric decay.

In an alternative approach, the observations may be explained in terms of a mixture of 1) Alfvén waves, created near the coronal base and propagating outward along the magnetic field lines, and 2) magnetic structures convected by the expanding wind.

In this regard, it should be stressed that the view of a bimodal character of the solar wind variability at MHD scales, with an Alfvénic turbulence propagating from quiet regions of the Sun and interspersed with highly filamentary structures convected from regions in the inner corona, is recently gaining evidence [2, 13, 14, 32]. Efforts in modeling solar wind fluctuations should strongly address this point.

Finally, it is certainly important to extend in-situ measurements to close-to-Sun regions. This is the aim of future missions as Solar Orbiter and Solar Probe. While the latter will have an extremely low perihelion ($\sim$ 4 solar radii), but with the drawback of a very quick passage, the former will be collecting data for long periods of time at ~ 0.2 AU in a nearly-heliosynchronous trajectory. This is a key advantage of Solar Orbiter. From this co-rotational vantage point the temporal and spatial variations of the solar wind can be disentangled unambiguously, enabling us to better understand the links between solar and heliospheric processes. More specifically, this will allow to clearly identify the different components of the solar wind variability.

Acknowledgements We are indebted to N. Gopalswamy, R. Ramesh, and K. E. Rangarajan for the invitation at the Asia-Pacific Regional School on Heliophysical Processes (Kodaikanal Observatory, Indian Institute of Astrophysics).

References

1. Barnes, A., in: Parker, E. N., Kennel, C. F., Lanzerotti, L. J. (eds.) Solar System Plasma Physics, vol. 1, p. 249, North-Holland, Amsterdam (1979)
2. Bavassano, B., Bruno, R., Ann. Geophys., 24, 3179 (2006)
3. Bavassano, B., Dobrowolny, M., Mariani, F., Ness, N. F., J. Geophys. Res., 87, 3617 (1982)
4. Bavassano, B., Pietropaolo, E., Bruno, R., J. Geophys. Res., 103, 6521 (1998)
5. Bavassano, B., Pietropaolo, E., Bruno, R., J. Geophys. Res., 105, 15,959 (2000)
6. Bavassano, B., Pietropaolo, E., Bruno, R., J. Geophys. Res., 106, 10,659 (2001)
7. Bavassano, B., Pietropaolo, E., Bruno, R., Ann. Geophys., 22, 689, (2004)
8. Bavassano, B., Bruno, R., Carbone, V., in: Poletto, G., Suess, S.T. (eds.) The Sun and the heliosphere as an integrated system, vol. 317, p. 253, Astrophysics and Space Science Library, Kluwer, Dordrecht (2004)
9. Belcher, J. W., Davis, L., Jr., J. Geophys. Res., 76, 3534, (1971)
10. Breech, B., Matthaeus, W. H., Minnie, J., Oughton, S., Parhi, S., Bieber, J. W., Bavassano, B., Geophys. Res. Lett., 32, L06103, doi:10.1029/2004GL022321 (2005)

11. Bruno, R., Carbone, V., The solar wind as a turbulence laboratory, in: Living Rev. Solar Phys. 2 (2005), http://www.livingreviews.org/lrsp-2005-4. Cited 15 March 2008
12. Bruno, R., Bavassano, B., and Villante, U., J. Geophys. Res., 90, 4373 (1985)
13. Bruno, R., DAmicis, R., Bavassano, B., Carbone, V., SorrisoValvo, L., Ann. Geophys., 25, 1913 (2007)
14. Chapman, S. C., Hnat, B., Geophys. Res. Lett., 34, L17103, doi:10.1029/2007GL030518 (2007)
15. Coleman, P. J., Jr., Astrophys. J., 153, 371, (1968)
16. D'Amicis, R., Bruno, R., Bavassano, B., Geophys. Res. Lett., 34, L05108, doi:10.1029/2006GL028896 (2007)
17. Denskat, K. U., Neubauer, F. M., J. Geophys. Res., 87, 2215 (1982)
18. Dobrowolny, M., Mangeney, A., Veltri, P., Phys. Rev. Lett., 45, 144, (1980)
19. Goldstein, B. E., Smith, E. J., Balogh, A., Horbury, T. S., Goldstein, M. L., Roberts, D. A., Geophys. Res. Lett., 22, 3393, (1995)
20. Horbury, T. S., Tsurutani, B. T., in: Balogh, A., Marsden, R. G., Smith, E. J. (eds.) The heliosphere near solar minimum: The Ulysses perspective, p. 167, Springer-Verlag, Berlin, (2001)
21. Horbury, T. S., Balogh, A., Forsyth, R. J., Smith, E. J., Geophys. Res. Lett., 22, 3401 (1995)
22. Horbury, T. S., Balogh, A., Forsyth, R. J., Smith, E. J., Astron. Astrophys., 316, 333 (1996)
23. Malara, F., Primavera, L., Veltri, P., Phys. Plasmas, 7, 2866 (2000)
24. Marsch, E. Tu, C.-Y., J. Geophys. Res., 95, 8211 (1990)
25. Matthaeus, W. H., Goldstein, M. L., Roberts, D. A., J. Geophys. Res., 95, 20,673 (1990)
26. Matthaeus, W. H., Zank, G. P., Smith, C. W., Oughton, S., Phys. Rev. Lett., 82, 3444 (1999)
27. Matthaeus, W. H., Minnie, J., Breech, B., Parhi, S., Bieber, J. W., Oughton, S., Geophys. Res. Lett., 31, L12803, doi:10.1029/2004GL019645 (2004)
28. McComas, D.J., Bame, S.J., Barraclough, B.L., Feldman, W.C., Funsten, H.O., Gosling, J.T., Riley, P., Skoug, R., Balogh, A., Forsyth, R., Goldstein, B.E., Neugebauer, M., Geophys. Res. Lett., 25, 1 (1998)
29. McComas, D. J., Elliot, H. A., Gosling, J. T., Reisenfeld, D. B., Skoug, R. M., Goldstein, B. E., Neugebauer, M., Balogh, A., Geophys. Res. Lett., 29(9), doi:10.1029/2001GL014164 (2002)
30. McComas, D. J., Elliott, H. A., Schwadron, N. A., Gosling, J. T., Skoug, R. M., Goldstein, B. E., Geophys. Res. Lett., 30(10), 1517, doi:10.1029/2003GL017136 (2003)
31. Neugebauer, M., Goldstein, B. E., McComas, D. J., Suess, S. T., Balogh, A., J. Geophys. Res., 100, 23,389 (1995)
32. Ogilvie, K. W., Coplan, M. A., Roberts, D. A., Ipavich, F., J. Geophys. Res., 112, A08104, doi:10.1029/2007JA012248 (2007)
33. Roberts, D. A., Goldstein, M. L., Klein, L. W., J. Geophys. Res., 95, 4203 (1990)
34. Roberts, D. A., Ghosh, S., Goldstein, M. L., Matthaeus, W. H., Phys. Rev. Lett., 67, 3741 (1991)
35. Schmidt, J. M., Ann. Geophys., 13, 475 (1995)
36. Schmidt, J. M. Marsch, E., Ann. Geophys., 13, 459 (1995)
37. Smith, E. J., Balogh, A., Neugebauer, M., McComas, D. J., Geophys. Res. Lett., 22, 3381 (1995)
38. Tu, C.-Y. and Marsch, E., J. Geophys. Res., 98, 1257 (1993)
39. Tu, C.-Y., and Marsch, E., Space Sci. Rev., 73, 1 (1995)
40. Vellante, M. and Lazarus, A. J., J. Geophys. Res., 92, 9893 (1987)